IET Renewable Power Generation

WILEY

IET The Institution of Engineering and Technology

ORIGINAL RESEARCH OPEN ACCESS

A Multi-Period Source-Storage Coordinated Planning Considering Locational Wind-Solar Complementarity and Dynamic Cost With Self-Declared Capacity

Yuankang He[2] | Zijun Mao[1] | Hongxing Ye[1]

[1]School of Automation Science and Engineering, Xi'an Jiaotong University, Xi'an, Shaanxi, China | [2]Department of Electrical Engineering, Xi'an Jiaotong University, Xi'an, Shannxi, China

Correspondence: Hongxing Ye (yehxing@xjtu.edu.cn)

Received: 26 November 2025 | **Revised:** 10 December 2025 | **Accepted:** 7 January 2026

ABSTRACT

With fast growing renewable generations, source-grid-load-storage (SGLS) integrated systems have emerged in recent years. The economical feasibility of SGLS system is still a challenge in many power systems. This paper proposes a multi-period source-storage coordinated planning model for SGLS system project considering spatio-temporal complementarity and dynamic source cost. In order to capture demand for flexible resource and wind-solar complementarity, the model develops hourly operation constraints for wind power, photovoltaic output, and load. It incorporates annually changing investment costs for photovoltaic generators, wind turbine, and energy storage, determining the optimal investment timing. A concept of self-declared capacity is proposed to coordinately minimize the capacity fee by leveraging local resources. Case study with real-data demonstrates that the proposed model can reduce total life-cycle costs by 7.54% to 9.67% and capacity costs by approximately 7.6%, compared to the original project, while assisting the main grid in peak shaving and valley filling. The results reveal that wind farms tends to be built in the early stages, while PV generator and energy storage tend to defer investments. A high proportion of PV generator has seen an increase in the share of energy storage, while energy storage is most sensitive to cost reductions.

1 | Introduction

The global energy transition towards sustainability is driving the rapid integration of renewable energy sources into power systems [1, 2]. The power system planning and operation tends to jointly coordinate sources, grids, loads, and storage, improving the utilization efficiency and unlocking flexibility of various resources. The source-grid-load-storage (SGLS) integrated system has emerged as a pivotal concept addressing this need. An SGLS system operates in a coordinated fashion, with a primary emphasis on realizing strong synergy and efficient integration among its components [3].

Research on the scheduling aspect of SGLS has already been conducted extensively [4–9]. Although these operational studies are crucial, they often assume a given system configuration. The planning stage, which determines the optimal type, size, and timing of component investments, is fundamentally important for ensuring the technical and economic viability of an SGLS system.

In SGLS-related planning studies, accurately characterizing wind and solar power generation remains a major challenge. Numerous studies have been dedicated to addressing the uncertainty of wind and solar power generation. Stochastic optimization is one of the commonly used methods, generating random scenarios

Abbreviations: SGLS, source-grid-load-storage; PV, photovoltaic; TOU, time-of-use.

of wind and solar by pre-setting parameter distributions [3, 10] or deep learning [11]. Robust optimization is also widely applied in the literature on power system planning and operation. It avoids probabilistic assumptions by defining an uncertainty set and finding a solution that remains feasible under the worst-case realization within this set [12–15]. Information gap decision (IGD) is also frequently employed to address this uncertainty [16, 17].

Some studies also employs deterministic inputs based on historical data to describe wind and solar power generation. However, to reduce computational complexity, these studies often generate typical scenarios through clustering methods [18–22] or use the annual aggregation parameter [23] to simulate wind and solar power generation.

Although these studies have made significant contributions to SGLS planning, whether in probabilistic scenarios, uncertainty sets, or typical scenarios after clustering, they tend to weaken the spatio-temporal characteristics and complementarity properties of wind and solar power generation. Another limitation of the aforementioned studies is that they typically assume static unit investment costs, which prevents planning decisions from achieving true economic efficiency.

To address these challenges, this paper proposes a multi-period source-storage coordinated planning model. The main contributions are as follows:

1. This work proposes a source-storage planning approach that considers locational wind-solar complementarity. In order to capture the flexibility demand, the hourly operation constraints are enforced in the planning model. The generation of PV and wind farms has seasonal trends and hourly profiles. The hourly operation constraints can capture the spatio-temporal and complementarity characteristics of local wind-solar resources.
2. A novel concept of self-declared capacity is proposed. In some electricity markets, such as China, the state holder of SGLS system pays the energy cost and the capacity fee. The capacity fee is calculated on the basis of the peak load. By leveraging local resources within SGLS, this work proposes to submit a self-declared peak load, which is a net peak load, that is, local generation minus load.
3. The model incorporates the dynamic investment cost of the renewable generator and storage. This helps determine the optimal investment time for different resources. Therefore, the state holder can minimize the life-cycle energy cost with optimally self-declared capacity, installed capacity for resources, and investment time.
4. This work conducts comprehensive case studies with real-world data from western China. By considering the locational wind-solar complementarity, self-declared capacity, and dynamic investment cost, the real-world data based simulation results provide insights for SGLS system planning. Some general inclusions can be applied in different regions.

The remainder of this paper is organized as follows. Section 2 analyzes the limitations of existing research in detail and proposes a source-storage operational mode; Section 3 constructs the multi-period source-storage coordinated planning model; Section 4 introduces the evaluation metrics for planning results; Section 5 analyzes optimal planning strategies under different cost reduction pathways and resource characteristics. Finally, this paper is concluded in Section 6.

2 | Problem Statement

This section will discuss the two issues raised in the Introduction section, and develop a source-storage coordinated optimization framework.

2.1 | Spatio-Temporal Characteristics of Wind and Solar Resources

As highlighted in the introduction, a significant challenge in SGLS planning lies in the accurate characterization of wind and solar power generation. The core of the problem is twofold. First, existing methods, whether based on random scenarios, uncertainty sets, or clustered typical scenarios, often struggle to accurately capture the full-resolution temporal characteristics of wind and solar generation. This limitation makes it difficult to represent critical operational details such as intra-hour variability, multi-day "wind droughts," or rapid ramping events, which are essential for determining storage sizing and system flexibility requirements. Second, solar generation peaks during daylight hours and wind generation often increases at night or in certain seasons. This inherent daily and seasonal complementarity between wind and solar resources is a valuable characteristic, which can be leveraged to reduce storage requirements and overall system costs. When this complementarity is diluted with aggregation or probabilistic representation, the planning model can fail to exploit this natural synergy for a more economical system design.

Against this problem, the model proposed in this paper calculates the instantaneous capacity factor based on 8760 h of historical wind and solar output data. By combining this with the planning wind and solar capacity, the maximum hourly output limit for wind and solar power can be determined.

This methodology ensures that the optimal planning strategy is performed against the exact chronological sequence of 8760 hourly data points for an entire year. By doing so, the model explicitly accounts for the precise timing of peak solar insolation, nocturnal wind patterns, and the correlation between resource availability and load demand. The resulting planning strategy is therefore deeply tailored to the unique temporal characteristics and complementarity properties of the local wind and solar resources, leading to a system configuration that is both more reliable and economically efficient than those derived from simplified representations.

2.2 | Investment Cost and Capacity Fee

A critical factor influencing the economics of source-storage coordinated planning is the rapid decline in the cost of key technologies. According to the "China Renewable Energy Project

Cost Management Report 2024" released by the China Renewable Energy Engineering Institute (CREEI), the total investment per kilowatt for centralized onshore photovoltaic power generation projects in China has significantly decreased from approximately 14,850 RMB/kW at the beginning of the 12th Five-Year Plan period (2011) to about 3,450 RMB/kW in 2024, representing a reduction of over 76%. During the same period, the unit cost of wind power projects has also been declining annually: In 2024, the onshore unit cost reached 4,200 RMB/kW, representing a decrease of approximately 49% compared to 2011. This rate of decline is slightly lower than that of photovoltaic projects. CREEI forecasts that investment costs for solar and wind power will decrease by approximately 25% and 20%, respectively, by 2030.

Equally important is the cost decline in energy storage, a key enabler for mitigating the intermittency of renewables. According to the report "Batteries and the Energy Security Transition" published by the International Energy Agency (IEA) in 2024, lithium-ion battery costs have fallen by 90% since 2010, with higher energy density and longer lifespans. Their price dropped from $1,400 per kWh in 2010 to under $140 per kWh in 2023, making it one of the fastest-declining energy technologies in terms of cost. IEA also forecasts that the cost of lithium-ion battery energy storage will decline by a further 30%–40% by 2030.

Existing single-period planning models are often based on static cost assumptions [10, 11, 18, 19]. While multi-period planning models incorporate discount factors, the unit investment costs for various facilities within the planning period are also treated as fixed parameters [13–16, 20]. Ignoring these dynamic cost trends prevents models from optimizing the crucial trade-off between "early investment for early returns" and "delayed investment for lower costs" across the project life-cycle—a strategic decision vital for the economic success of SGLS system projects.

To implement these insights, this model sets the unit investment costs for wind turbines, PV generators, and energy storage as dynamic parameters that decline annually at a fixed rate, with the decline rate calculated based on reports from CREEI and IEA. In the meantime, the capacity is considered as a decision variables. The model can effectively balance the benefit of early revenue generation against the advantage of accessing cheaper technologies in future years, thereby achieving truly economically optimal planning decisions that reflect real-world market dynamics.

2.3 | Self-Declared Capacity Fee

The capacity fee is the payment made by the state holder of the SGLS system to the main grid in some electricity markets. The capacity fee is collected to guarantee the peak-load supply by the main grid. Therefore, it is calculated based on the peak load level of the market participants. As a new market participant, the SGLS system can adjust the net load by adjusting the local generators and storage, even the loads. Therefore, it provides an opportunity to self-declare capacity.

When self-declared capacity is incorporated into the planning model, SGLS system owners can further reduce lifecycle costs. Simultaneously, under capacity cost constraints, they can also minimize their maximum demand to reduce the impact on the main grid.

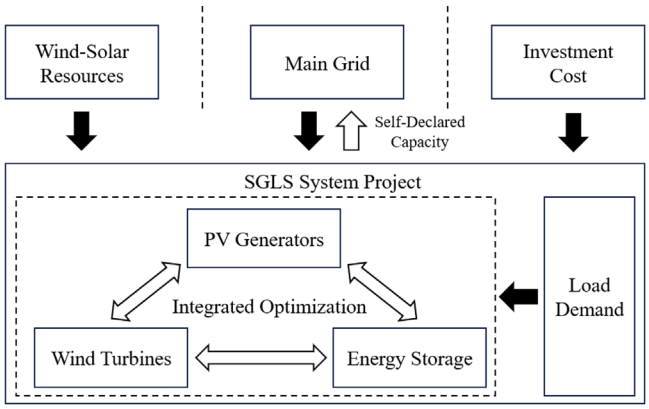

FIGURE 1 | Schematic diagram of source-storage coordinated planning.

2.4 | Framework of Source-Storage Coordinated Planning

Beyond accurate wind-solar representation and dynamic costs, a credible planning model must consider realistic operation scenarios. The SGLS system does not operate in isolation but interacts continuously with the main grid. Based on the preceding analysis, this subsection proposes a framework of source-storage coordinated planning for the SGLS system project.

The proposed framework of source-storage coordinated planning, as illustrated in Figure 1, considers a generation-side consisting exclusively of wind turbines and PV generators (most relevant to the modern power system [24]), complemented by energy storage system and connected to the main grid to serve the local load demand.

This schematic highlights the multiple, interacting factors that the planning model must consider:

- **Wind-Solar Resources**: The spatio-temporal characteristics of local wind and solar resources play a critical role in shaping system planning. Wind power typically peaks at night, whereas solar generation is concentrated during daytime hours, giving rise to natural complementarity that significantly affects the optimal capacity allocation among wind, PV, and storage.
- **Main Grid**: While the generation side contains only intermittent renewable sources, the project inevitably relies on the main grid to purchase electricity during periods of resource shortfall, ensuring reliable supply to the internal load. This interaction imposes dual requirements: the project must achieve both internal economic efficiency and stable operation while simultaneously satisfying grid-support obligations. These include smoothing the net load curve of the main grid, reducing peak downward power flows to prevent transmission overloads, and providing peak-shaving and valley-filling services, collectively enhancing overall grid-friendliness. In

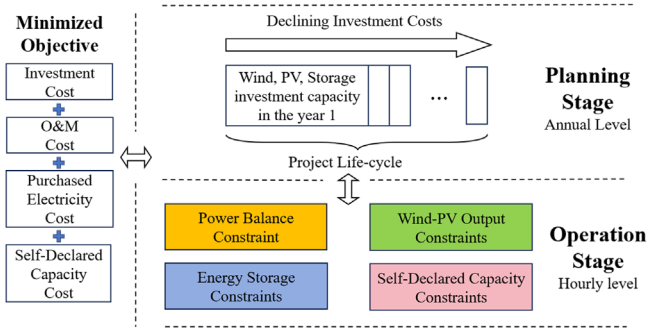

FIGURE 2 | Structure of the proposed model.

return, the state holder of SGLS system has the opportunity to pay less for capacity fee.

- **Investment Cost**: The markedly different capital costs of wind turbines, PV generators, and energy storage, combined with their distinct annual cost-decline trajectories, constitute a critical economic driver. The optimization must strategically balance installed capacities and investment timing across technologies to minimize the net present value of the life-cycle cost.
- **Load Demand**: The shape and characteristics of the internal load profile play an equally important role. Industrial-dominated loads with relatively flat daily patterns tend to pair better with wind-rich resources for example. Consequently, the optimal wind-PV-storage planning is highly sensitive to both resource availability and the specific load curve of the project.

By explicitly incorporating these four factors, the proposed multi-period planning model delivers a tailored, economically optimal, and grid-friendly source-storage planning for renewable-dominated SGLS systems.

3 | Multi-Period Source-Storage Coordinated Planning Model

This section proposes a multi-period source-storage coordinated planning model. The model accounts for the annual decreasing trend in investment costs for renewable generation and energy storage systems, while embedding deterministic hourly wind power output, photovoltaic output data, and load data into the constraints. Figure 2 illustrates the structure of proposed model.

As shown in Figure 2, the proposed model adopts a classic two-stage planning-operation framework. At the planning stage, annual decisions are made to determine the newly added installed capacities of wind turbines, PV generators, and energy storage systems for each year of the project life-cycle. The operation stage operates on an hourly basis, optimizing hourly wind and solar output, energy storage charge/discharge power, and purchased electricity from main grid. Through interaction between the two stages, the model derives the capacity planning path for wind, solar, and storage that minimizes NPV, along with the corresponding operational plan.

3.1 | Objective Function

The planning model aims to minimize the net present value (NPV) of the total life-cycle cost while ensuring reliable operation and grid compatibility. Under the SGLS operation model, costs primarily consist of investment cost, operation and maintenance cost, purchased electricity cost, and self-declared capacity cost. The objective function is formulated as:

$$\min \sum_{y \in Y} \frac{1}{(1+r)^y} \left\{ C_y^I + C_y^{OM} + C_y^E + C_y^C \right\} \tag{1}$$

where Y represents the project lifespan (in years); C_y^I, C_y^{OM}, C_y^E and C_y^C represent the investment cost, operation and maintenance cost, purchased electricity cost, and self-declared capacity cost in year y, respectively; r is the discount rate; $\frac{1}{(1+r)^y}$ is the present value factor for year y.

3.1.1 | Investment Cost

The investment cost accounts for the capital expenditure of deploying new capacities each year, considering the factor of declining investment costs:

$$C_y^I = c_y^{pv} \cdot \Delta P_y^{pv} + c_y^{wind} \cdot \Delta P_y^{wind} + c_y^{sto} \cdot \Delta E_y^{sto} \tag{2}$$

where ΔP_y^{pv}, ΔP_y^{wind} and ΔE_y^{sto} denote the newly installed capacities of PV generator, wind turbine, and energy storage in year y; c_y^{pv}, c_y^{wind} and c_y^{sto} are the unit investment costs in year y.

According to reports released by CREEI and IEA, the unit cost trend for wind turbine, photovoltaic generator, and lithium energy storage has exhibited an exponential decline over the past decade. Therefore, the annual decline rate is employed here to approximate the yearly changes in the investment costs per unit for these technologies:

$$c_y^{pv} = c_0^{pv} \cdot (1 - d_{pv})^y \tag{3}$$

$$c_y^{\text{wind}} = c_0^{\text{wind}} \cdot (1 - d_{\text{wind}})^y \tag{4}$$

$$c_y^{\text{sto}} = c_0^{\text{sto}} \cdot (1 - d_{\text{sto}})^y \tag{5}$$

where d_{pv}, d_{wind} and d_{sto} represent the annual decline rates of investment costs for PV generator, wind turbine, and energy storage, respectively.

3.1.2 | Operation and Maintenance Cost

The O&M cost comprises fixed O&M costs and battery replacement costs of ESS:

$$C_y^{OM} = C_y^{fixed} + C_y^{rep} \tag{6}$$

$$C_y^{fixed} = om_y^{pv} \cdot P_y^{pv} + om_y^{wind} \cdot P_y^{wind} + om_y^{sto} \cdot P_y^{sto} \tag{7}$$

$$C_y^{rep} = rep_y \cdot \Delta P^{sto}_{y-Y^{sto}} \tag{8}$$

where om_y^{pv}, om_y^{wind} and om_y^{sto} are the unit fixed O&M costs; $P_y^{pv}, P_y^{wind} and P_y^{sto}$ are the cumulative installed capacities in year y; C_y^{rep} is the unit battery replacement cost, which can generally be considered a fixed proportion of the investment unit cost ESS; $\Delta P^{sto}_{y-Y^{sto}}$ is the ESS capacity added in year $y - Y^{sto}$, with Y^{sto} being the ESS service life.

3.1.3 | Purchased Electricity Cost

The purchased electricity cost represents the expense of purchasing electricity from the main grid:

$$C_y^E = \sum_{t \in T} \pi_{t,y} \cdot p_{t,y}^M \tag{9}$$

where $T = 8760$ is the total number of hours in a year, $\pi_{t,y}$ is the time-of-use (TOU) electricity price published by the local government (typically divided into peak, flat, and valley periods), and $p_{t,y}^M$ is the electricity purchased from the main grid at hour t of year y.

By explicitly incorporating real-world TOU pricing into the hourly operational constraints, the model naturally incentivizes valley-period electricity procurement (when prices are lowest) and peak-period purchased reduction (when prices are highest). This economically driven behavior not only reduces the project's own electricity expenditure, but simultaneously delivers significant grid-support benefits: increased valley filling and reduced peak downward power flow effectively smooth the net load curve seen by the main grid, lower the system's peak regulation pressure, and enhance overall grid-friendliness without requiring additional control or incentive mechanisms.

3.1.4 | Self-Declared Capacity Cost

To ensure compatible operation and maintain a stable connection between the SGLS system project and the main grid, the SGLS system must declare its maximum demand capacity in a year to the grid operator and pay the corresponding capacity fee. This grid-friendly approach helps prevent overload at the grid connection and ensures reliable power exchange:

$$C_y^C = \pi_y^{cap} \cdot MD_y \tag{10}$$

where π_y^{cap} is the capacity price; MD_y is the declared maximum demand capacity, which represents the SGLS system project's commitment to not exceed this power level when purchasing electricity from the main grid, thereby supporting grid stability and facilitating friendly grid integration.

3.2 | Constraints for the Planning Stage

Constraints for the planning stage impose restrictions on the decision variables for the multi-period planning problem, which are shown in (11)-(14):

For each year y, the capacity expansion must be non-negative:

$$\Delta P_y^{\mathrm{pv}} \geq 0, \quad \Delta P_y^{\mathrm{wind}} \geq 0, \quad \Delta E_y^{\mathrm{sto}} \geq 0 \tag{11}$$

The cumulative capacities follow a recursive relationship:

$$rClP_y^{\mathrm{pv}} = P_{y-1}^{\mathrm{pv}} + \Delta P_y^{\mathrm{pv}} \tag{12}$$

$$P_y^{\mathrm{wind}} = P_{y-1}^{\mathrm{wind}} + \Delta P_y^{\mathrm{wind}} \tag{13}$$

$$E_y^{\mathrm{sto}} = E_{y-1}^{\mathrm{sto}} + \Delta E_y^{\mathrm{sto}} \tag{14}$$

with initial conditions P_0^{pv}, P_0^{wind} and $E_0^{\mathrm{sto}} = 0$

3.3 | Constraints for the Operation Stage

Constraints for the operation stage impose restrictions on the decision variables for the operation problem, which are presented as follows:

For each year y and each hour t, the following operational constraints ensure reliable SGLS system operation:

$$p_{t,y}^{pv} + p_{t,y}^{\mathrm{wind}} + p_{t,y}^{st} + p_{t,y}^{M} = D_{t,y} \tag{15}$$

$$0 \leq p_{t,y}^{\mathrm{pv}} \leq \rho_{t,y}^{\mathrm{pv}} \cdot P_y^{\mathrm{pv}} \tag{16}$$

$$0 \leq p_{t,y}^{\mathrm{wind}} \leq \rho_{t,y}^{\mathrm{wind}} \cdot P_y^{\mathrm{wind}} \tag{17}$$

$$SOC_{\min} \cdot E_y^{\mathrm{sto}} \leq E_{t,y} \leq SOC_{\max} \cdot E_y^{\mathrm{sto}} \tag{18}$$

$$p_{t,y}^{\mathrm{st}} = p_{t,y}^{\mathrm{dis}} - p_{t,y}^{\mathrm{ch}} \tag{19}$$

$$rClp_{t,y}^{\mathrm{ch}} \leq P_y^{\mathrm{sto}} \tag{20}$$

$$p_{t,y}^{\mathrm{ch}} \leq \frac{SOC_{\max} \cdot E_y^{\mathrm{sto}} - E_{t-1,y}}{\eta_{\mathrm{ch}}} \tag{21}$$

$$p_{t,y}^{\mathrm{ch}} \geq 0 \tag{22}$$

$$p_{t,y}^{\mathrm{dis}} \leq P_y^{\mathrm{sto}} \tag{23}$$

$$p_{t,y}^{\mathrm{dis}} \leq \eta_{\mathrm{dis}} \cdot (E_{t-1,y} - SOC_{\min} \cdot E_y^{\mathrm{sto}}) \tag{24}$$

$$p_{t,y}^{\mathrm{dis}} \geq 0 \tag{25}$$

$$E_{t,y} = E_{t-1,y} + \eta_{\mathrm{ch}} \cdot p_{t,y}^{\mathrm{ch}} - \frac{p_{t,y}^{\mathrm{dis}}}{\eta_{\mathrm{dis}}} \tag{26}$$

$$\mathrm{MD}_y \geq p_{t,y}^{M} \tag{27}$$

$$p_{t,y}^{M} \geq 0 \tag{28}$$

In the above formulation, Equation (15) is the power balance constraint, where $p_{t,y}^{pv}$, $p_{t,y}^{wind}$, $p_{t,y}^{sto}$, $p_{t,y}^{M}$ and $D_{t,y}$ represent the photovoltaic output, wind power output, net energy storage discharge

power, purchased electricity, and load power at time t in year y, respectively, and the load is a fixed input data; Equations (16) and (17) are the renewable generation constraint, where $\rho_{t,y}^{pv} \cdot P_{t,y}^{pv}$ and $\rho_{t,y}^{wind} \cdot P_{t,y}^{wind}$, respectively, denote the maximum upper limits of available PV and wind power output at time t in year y. These limits can be obtained by multiplying the PV capacity factor $\rho_{t,y}^{pv}$ and wind capacity factor $\rho_{t,y}^{wind}$ at time t in year y by the installed capacity of PV and wind power, respectively. $\rho_{t,y}^{pv}$ and $\rho_{t,y}^{wind}$ represent the ratio of historical actual output data to rated installed capacity for wind turbines and photovoltaic generator, respectively.

Equations (18)–(26) are the ESS operational constraints where $p_{t,y}^{\mathrm{dis}}$ and $p_{t,y}^{\mathrm{ch}}$ denote the energy discharge power and energy charge power at time t in year y, respectively; $P_y^{\mathrm{sto}} = E_y^{\mathrm{sto}}/\beta$ denotes the rated power of the energy storage, where β represents the duration of the energy storage; η_{ch} and η_{dis} denote the charging and discharging efficiency of the energy storage; Equations (20)–(22) are the energy storage charging constraint: charging power is less than the rated power and the remaining chargeable capacity; Equations (23)–(25) are the energy storage discharge constraint: the discharge power must be less than the rated power and the remaining available capacity. Equations (18) and (26) are, respectively, the SOC constraint for energy storage and the energy balance constraint; Equations (27) and (28) are the self-declared capacity constraints, which ensures the declared annual maximum demand capacity MD_y covers the actual maximum power drawn from the grid in this year, supporting grid-friendly operation.

It can be observed that the proposed model is a mixed integer linear programming problem. It can be solved using commercial or open-source optimization solvers. The multi-period approach allows for adaptive planning that responds to changing investment costs and operational requirements throughout the project life-cycle.

4 | Evaluation Metrics

This section introduces a set of metrics to measure the planning results of the proposed multi-period source-storage model, encompassing both economic and grid friendliness.

4.1 | Cost Efficiency

The purpose of this subsection is to quantify the optimization effects of the model on the NPV of the full life-cycle costs, comparing original project and optimized scenarios.

Key indicators include:

- **Life-Cycle Cost Savings Ratio**: This evaluates the percentage reduction in costs before and after optimization.

$$\frac{NPV_{ori} - NPV_{opt}}{NPV_{ori}} \times 100\% \tag{29}$$

where NPV_{ori} is the NPV of total cost of the original project and NPV_{opt} is the NPV of total cost of the optimized project.

- **Self-Declared Capacity Cost Savings Ratio**: This evaluates the percentage reduction in costs before and after optimization.

$$\frac{C_{ori}^{C} - C_{opt}^{C}}{C_{ori}^{C}} \times 100\% \tag{30}$$

where C_{ori}^{C} are the capacity costs of the original project and C_{opt}^{C} are the capacity costs of the optimized project. The reduction in capacity costs indicates that the SGLS system has decreased net peak-load and increased self-consumption rates.

4.2 | Grid Friendliness

The purpose of this subsection is to evaluate grid-friendliness of the model based on 8760 h operational data.

Key indicators include:

- **Maximum Dependence Reduction Ratio (MDRR)**: This quantifies the reduction in maximum dependence on the main grid after optimization, reflecting peak value reduction to avoid overloads.

$$MDRR = \frac{1}{Y} \sum_{y} \frac{MD_{ori} - MD_{y}}{MD_{ori}} \times 100\%$$

where MD_y is the maximum dependence power from the main grid in year y in the optimized scheme, and MD_{ori} is in the original scheme. The maximum is taken over the year. A higher value indicates greater grid-friendliness.

- **Peak Reduction Ratio (PRR)**: This quantifies the model contribution to peak shaving (reducing purchases during the peak load period of the main grid), helping smooth the main grid's load curve.

$$PRR = \frac{\sum_{t \in peak} (P_{t,ori}^{M} - P_{t,opt}^{M})}{\sum_{t \in peak} P_{t,ori}^{M}} \times 100\%$$

where *peak* is the set of peak periods which is determined by the locally published electricity pricing periods.

- **Valley Filling Ratio (VFR)**: This quantifies the SGLS system contribution to valley filling (increasing purchases during the valley load period of the main grid), helping smooth the main grid's load curve.

$$VFR = \frac{\sum_{t \in valley} (P_{t,opt}^{M} - P_{t,ori}^{M})}{\sum_{t \in valley} P_{t,ori}^{M}} \times 100\%$$

where *valley* is the set of valley periods which is also determined by the locally published electricity pricing periods.

5 | Case Study

This section uses a park-level SGLS system project in Xinjiang, China as a case study. It is equipped with 10 MW of PV generators, 350 MW of wind turbines, 60 MW/120 MWh of lithium battery

TABLE 1 | Economic parameters of SGLS project.

Devices	Unit investment cost (RMB/kW)	O&M cost (RMB/kW/y)
PV	3450	30
Wind	4200	40
Storage	1273*	20

*Unit: RMB/kWh for energy storage investment cost

TABLE 2 | Technical parameters of ESS.

Parameter	Value
Charging efficiency	95%
Discharging efficiency	95%
Storage duration	2 h
SOC upper limit	100%
SOC lower limit	0%
Battery replacement cost (% of ES)	60%

energy storage, and 340 MW peak load. This project is served as benchmark. We collect annual wind power, PV generation, and load data for 8760 h in 2024 as input for the model. Following local policy requirements, surplus electricity cannot be fed into the grid, and the energy storage system cannot participate in the ancillary service market, making it suitable for validation and analysis using the model proposed in this paper. Currently, there are no plans for load expansion in this project. As it does not participate in the energy market, the real-time electricity price is based on the local government's publicly announced time-of-use proxy electricity prices for January to December, and the capacity price is 360 RMB per kWh per year. It is assumed that the wind power and PV output characteristics, load curve, and proxy electricity price in the project area remain the same as in 2024 throughout the entire life-cycle. The project duration is 20 years, with a discount rate of 8%. Other economic parameters are shown in Table 1, and technical parameters of ESS are shown in Table 2. All parameters are obtained from publicly available reports and the project. This study uses Python 3.12.4 for model development and calls the Gurobi 12.0.2 optimization solver for the solution. All computations are performed on a computer equipped with an Intel Core i5-13600K processor and 32 GB of RAM.

5.1 | Optimal Planning Under Different Technological Cost Reduction Pathways

This section investigates the impact of cost reduction pathway uncertainty on life-cycle optimal planning by establishing three distinct annual cost reduction pathways (conservative, base, and optimistic) for photovoltaic generator, wind turbine, and energy storage. The base pathway ($d_{pv} = 5\%$, $d_{wind} = 4\%$, $d_{sto} = 7\%$) is defined based on the projections of CREEI and IEA for the unit cost of wind turbine, photovoltaic generator, and lithium energy storage in 2030. A conservative pathway ($d_{pv} = 3.5\%$, $d_{wind} = 2.5\%$, $d_{sto} = 5.0\%$) is formulated to represent potential headwinds such as slowed technological advancement, supply chain bottlenecks, and weaker policy support. Conversely, an optimistic pathway ($d_{pv} = 6.5\%$, $d_{wind} = 5.5\%$, $d_{sto} = 9\%$) assumes favorable conditions like accelerated technological breakthroughs, rapid supply chain cost reduction, and strong policy drivers. A static cost scenario with no reduction is also included as a benchmark. A comparative analysis is conducted from the perspectives of investment timing, technology portfolio, and system costs to evaluate the robustness of the planning strategy against technological cost uncertainty, providing insights for medium-term and long-term source-storage coordinated planning.

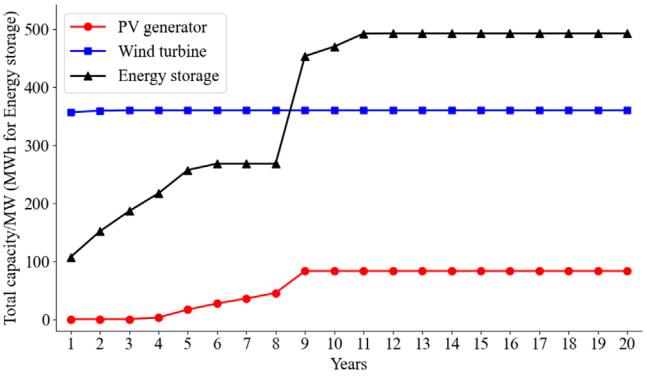

FIGURE 3 | Life-cycle capacity expansion under the base cost reduction pathway.

1. **Base Cost Reduction Pathway** ($d_{pv} = 5\%$, $d_{wind} = 4\%$, $d_{sto} = 7\%$): Under the base pathway, the unit investment costs for photovoltaic generator, wind turbine, and energy storage are projected to decrease to approximately 81%, 85%, and 75% of the base-year costs by Year 5, and further to 63%, 69%, and 52% by Year 10, respectively.
   Figure 3 illustrates the resulting capacity expansion strategy. The capacity of the PV generator increases steadily from Year 5 to Year 9, reaching a cumulative capacity of 83.1 MW before stabilizing. Wind turbine investment occurs primarily in the base year (356.9 MW), with a minor addition in Year 2 (reaching 360.3 MW), resulting in a wind-to-PV capacity ratio of approximately 4.3:1. Energy storage is deployed in phases from Year 1 to Year 11, achieving a final capacity of 492.9 MWh. The initial investment in energy storage in the base year constitutes 21.7% of the final capacity. The final storage-to-generation power capacity ratio is about 1.1:1. No further investments are made after Year 11.
2. **Conservative Cost Reduction Pathway** ($d_{pv} = 3.5\%$, $d_{wind} = 2.5\%$, $d_{sto} = 5.0\%$): Under the conservative pathway, costs decrease more slowly, reaching 87%, 90%, and 81% of base-year costs by Year 5, and 73%, 80%, and 63% by Year 10 for photovoltaic generator, wind turbine, and energy storage, respectively.
   As shown in Figure 4, the capacity of the PV generator is added gradually between Years 3 and 9, stabilizing at 50.3 MW. Capacity of wind turbine is installed almost entirely in the base year (361.8 MW), leading to a higher wind-to-PV ratio of 7.2:1. Energy storage is deployed in phases until Year 9, starting with 172.4 MWh in the base year (40.9% of the final 421.6 MWh capacity), with subsequent additions in Year 4 and Year 9. The final storage-to-generation ratio is nearly 1:1. The system stabilizes after Year 9.

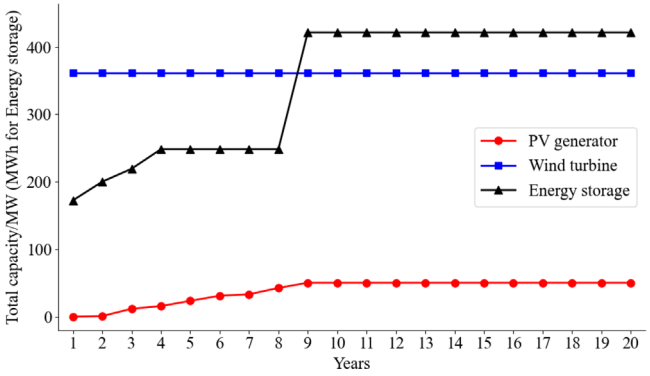

FIGURE 4 | Life-cycle capacity expansion under the conservative cost reduction pathway.

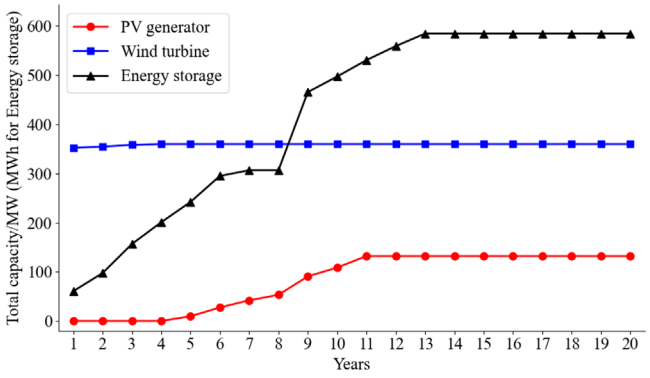

FIGURE 5 | Life-cycle capacity expansion under the optimistic cost reduction pathway.

3. **Optimistic Cost Reduction Pathway** ($d_{pv} = 6.5\%, d_{wind} = 5.5\%, d_{sto} = 9\%$): Under the optimistic pathway, significant cost reductions are realized, with costs falling to 76%, 80%, and 69% by Year 5, and 55%, 60%, and 43% by Year 10.
   Figure 5 shows a more deferred and expansive investment strategy. The capacity of the PV generator is added annually from Year 5 to Year 11, reaching a significantly higher final capacity of 132 MW. Wind investment occurs in the base year (352 MW) and Year 4 (reaching 359.7 MW), resulting in a lower wind-to-PV ratio of 2.7:1. The energy storage deployment is phased over a longer period until Year 13, reaching a final capacity of 584.4 MWh. Notably, only 10.3% of the final capacity of energy storage is installed in the base year, reflecting a strong deferral strategy. The final storage-to-generation ratio is 1.2:1. The system stabilizes after Year 13.
4. **Static Cost Scenario (No Reduction)**: For comparison, under the static cost assumption, the optimal strategy involves a single, upfront investment in the first year: 15.9 MW of PV generator, 363.5 MW of wind turbine, and 249.8 MWh of energy storage. No further capacity is added throughout the project life-cycle.

A comparative analysis of the planning decisions under the three dynamic pathways and the static scenario yields the following key insights:

1. The wind turbine serves as the primary generation source across all scenarios. Investments are concentrated in the early years, with minimal variation in final capacity (less than 0.4% difference between scenarios). This indicates that the planning decision for the capacity of the wind turbine is relatively insensitive to the examined range of its own cost reduction rates, likely due to its superior resource availability and economic viability in this specific project context.
2. In contrast, the capacity expansion of the PV generator demonstrates high sensitivity to cost reduction rates. Investments are consistently deferred until at least Year 3. The final capacity of the PV generator varies significantly: 50.3 MW (conservative), 83.1 MW (base), and 132 MW (optimistic). This 162% increase from the conservative to the optimistic scenario highlights PV generator's role as a flexible resource, whose investment timing and scale can be dynamically adjusted based on actual cost reduction trajectories.
3. Energy storage capacity is highly sensitive to cost reduction rates, both in terms of final capacity and investment phasing. The final capacity of energy storage is 421.6 MWh (conservative), 492.9 MWh (base), and 584.4 MWh (optimistic), corresponding to 102%, 111%, and 119% of the total generation capacity, respectively. Furthermore, the share of the capacity of energy storage installed in the base year decreases significantly as cost reductions become steeper (40.9%, 21.7%, and 10.3%, respectively), indicating a stronger tendency to defer investments when future costs are expected to be lower. This phasing also aligns with the battery replacement cycle, favoring later investments to reduce the net present cost of replacement.
4. The static cost scenario results in a significantly smaller and entirely front-loaded investment (15.9 MW PV generator, 249.8 MWh energy storage), failing to capture the flexibility and economic potential offered by future cost reductions, particularly for the PV generator and energy storage. This underscores the importance of incorporating dynamic cost projections in long-term planning.

5.2 | Assessment of Planning Results

This subsection will conduct an assessment of the planning results for different scenarios outlined in the preceding subsection, based on the evaluation metrics designed in Section 4.

1. **Life-Cycle Cost Savings Ratio**: The original project incurred an investment cost of 1.657 billion RMB in the base year (2024), with annual O&M costs of 0.0155 billion RMB, annual capacity costs of 0.12 billion RMB, and annual purchased electricity costs of 0.314 billion RMB. Based on these figures, the total life-cycle cost NPV for the original project is calculated to be 6.435 billion RMB (The cost of battery replacement in the 12th year is estimated based on the base cost reduction pathway of 7%). Figure 6 illustrates the NPV of total costs across the five scenarios.
   As shown in Figure 6, the optimal capacity planning derived from the model reduces the total cost NPV by 7.54% even under the static Cost assumption (no future cost reductions). When technological cost reductions are incorporated, the

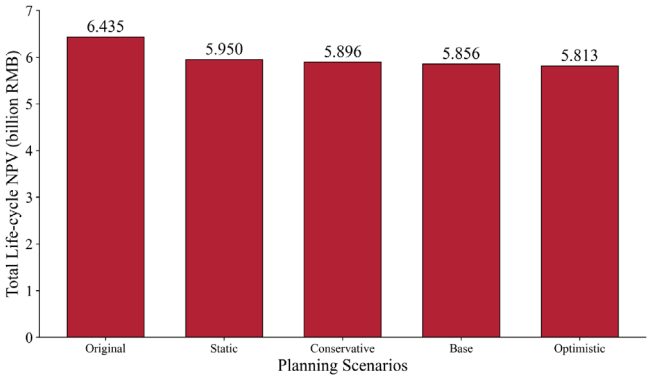

FIGURE 6 | NPV of total costs in different scenarios.

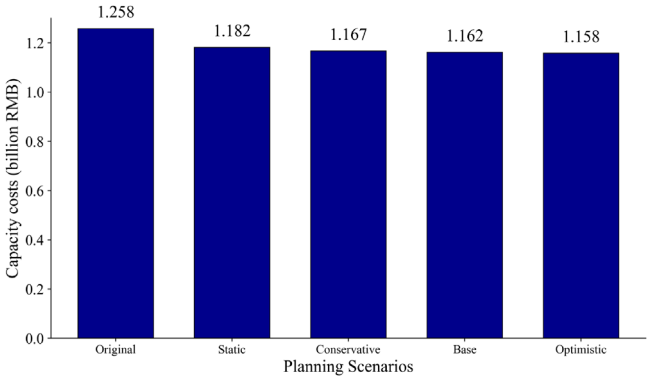

FIGURE 7 | Self-declared capacity costs in different scenarios.

TABLE 3 | Grid-friendly assessments in different scenarios.

Scenario	MDRR[1]	PRR[2]	VFR[3]
Static	6.2	40.3	34.1
Conservative	9.6	50.7	38.9
Base	10.3	53.4	37.3
Optimistic	11.1	55.8	33.3

[1]Maximum Dependence Reduction Ratio
[2]Peak Reduction Ratio
[3]Valley Filling Ratio

total cost NPV savings increase to 8.38%, 9.31%, and 9.67% for the conservative, base, and optimistic pathways, respectively, reflecting the economic benefits of deferred investment after accounting for cost reductions.

2. **Self-Declared Capacity Cost Savings Ratio Assessments**: The present value of the full-cycle capacity cost for the original project is 0.12 billion RMB. Figure 7 illustrates the capacity cost in different scenarios.
   As shown in Figure 7, without factoring in cost reductions, capacity costs decreased by 6.0%. When cost reductions are taken into account, this rate increases to approximately 7.6%. This indicates that the model can reduces the project's own net peak-load.
3. **Grid-Friendly Assessments**: Table 3 presents the grid-friendly assessments values of optimization results under four distinct optimization scenarios.

As shown in Table 3, in the scenario without cost reduction, the MDRR is 6.2%. Under the three cost reduction pathways, the MDRR increases to a range of 9.6% to 11.1%, showing a clear upward trend as costs decrease. This indicates that the model effectively reduces maximum power dependence on the main grid, with greater cost reductions leading to stronger grid autonomy.

Even without cost reduction, the model achieves a PRR of 40.3%, demonstrating considerable inherent peak-shaving capability. When cost reduction mechanisms are introduced, the PRR improves significantly from 50.7% to 55.8%, highlighting the model's enhanced ability to support grid load management during peak periods.

Across all four scenarios, the VFR remains between 33.3% and 38.9%, confirming the model's consistent contribution to valley filling. It is worth noting that the VFR does not exhibit a clear correlation with the degree of cost reduction, suggesting that valley filling performance is influenced more by operational strategies than by cost factors.

The results underscore the strong grid-friendly performance of the proposed model. It contributes notably to peak shaving and valley filling, thereby helping to flatten the load profile of the main grid, improve operational stability, and enhance overall economic efficiency. This performance is intrinsically linked to the optimal planning pathway identified earlier, where the significant expansion of energy storage capacity enables the system to purchase electricity extensively during the grid's load valleys—storing it for later use—while reducing grid purchases during peak hours by discharging the stored energy. This operational strategy not only minimizes electricity costs and improves the project's economic viability, but also supports the main grid in alleviating congestion, balancing supply-demand fluctuations, and reducing the need for peak-shaving power plants, thereby contributing to a more efficient and resilient power system.

5.3 | Optimal Capacity Planning Under Different Wind-Solar Resource Characteristics

Optimal source-storage capacity coordinated planning strategies for SGLS system project must be tailored to local wind and solar resource characteristics, which vary significantly across regions. To analyze optimal planning strategies under different wind and solar resource conditions, while validating the adaptability of the proposed model to diverse resource scenarios, this section utilizes an open dataset comprising field-measured data from renewable power plants in China [25]. The dataset includes 15-min interval generation and meteorological data from 2020 for six wind farms and eight PV plants, located across North, Central, and Northwest China, covering diverse terrains (desert, mountainous, plain) and climatic zones. By selecting specific combinations of wind and PV plants with distinct resource profiles, we simulate the power generation characteristics of regions with different resource characteristic and derive their corresponding optimal capacity plans. Tables 4 and 5 summarize the key operational characteristics of the selected wind farms and PV plants, respectively.

TABLE 4 | Operational characteristics of wind farms.

Site ID	Rated capacity (MW)	Average power (MW)	Capacity factor	Hub height wind speed (m/s)
1	99	23.4	0.24	6.4
2	200	72.7	0.36	7.5
3	99	18.1	0.18	4.0
4	66	17.4	0.26	5.5
5	36	6.7	0.19	4.7
6	96	28.8	0.30	8.1

TABLE 5 | Operational characteristics of PV plants.

Site ID	Rated capacity (MW)	Average power (MW)	Capacity factor	Total irradiance (W/m^2)
1	50	9.7	0.19	266.4
2	130	19.6	0.15	169.6
3	30	5.2	0.17	81.1
4	130	16.5	0.13	150.1
5	110	14.5	0.13	164.3
6	35	6.4	0.18	244.1
7	30	5.4	0.18	206.8
8	30	4.2	0.14	163.2

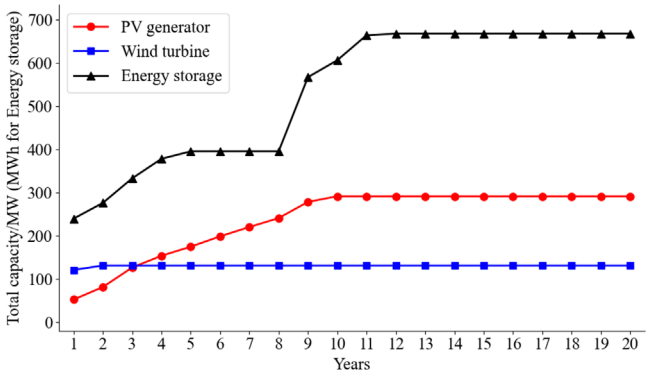

FIGURE 8 | Optimal capacity plan for the PV-dominant region.

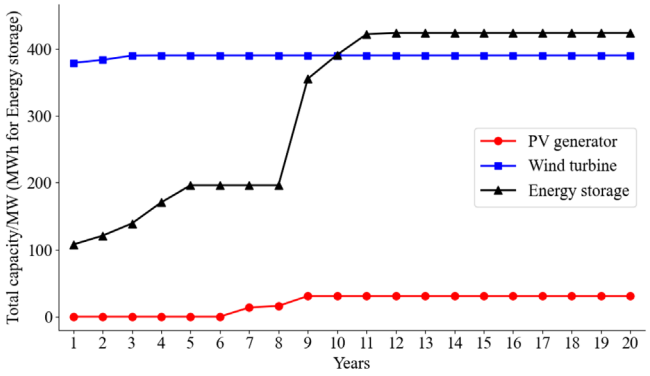

FIGURE 9 | Optimal capacity plan for the wind-dominant region.

Based on the capacity factors and hub-height wind speeds in Table 4, Wind Farms 2 and 6 are identified as resource-rich, while Farms 3 and 5 are resource-poor. Similarly, based on capacity factors and total irradiance in Table 5, PV Plants 1, 6, and 7 are considered resource-rich, whereas Plants 2, 4, and 5 are resource-poor. This classification allows us to simulate three typical resource endowment profiles: PV-dominant, wind-dominant, and balanced wind-solar. The load profile and other technical/economic parameters remain consistent with Section 3.1. The base cost reduction pathway ($d_{pv} = 5\%$, $d_{wind} = 4\%$, $d_{sto} = 7\%$) is applied.

1. **PV-Dominant Region**: A PV-dominant region is simulated using resource-rich PV Plant 1 and resource-poor Wind Farm 5. The resulting optimal life-cycle capacity expansion plan is shown in Figure 8.

As shown in Figure 8, the optimal strategy involves an initial investment for PV generator of 52.3 MW in the first year, followed by gradual annual expansion, reaching a cumulative capacity of 291.5 MW by Year 10. The capacity of the wind turbine is fully deployed within the first 2 years, totaling 131.1 MW, resulting in a final wind-to-PV capacity ratio of 0.45:1. Energy storage starts with 239.6 MWh in Year 1 and expands to 664.3 MWh by Year 9. The final storage-to-generation power capacity ratio is 1.57:1. This high ratio is necessary because PV generation, being the primary source, is highly intermittent on a diurnal cycle, requiring significant energy storage to shift energy from daytime production to meet evening peak load demand.

2. **Wind-Dominant Region**: A wind-dominant region is simulated using resource-rich Wind Farm 2 and PV Plant 1. The optimal plan is shown in Figure 9.

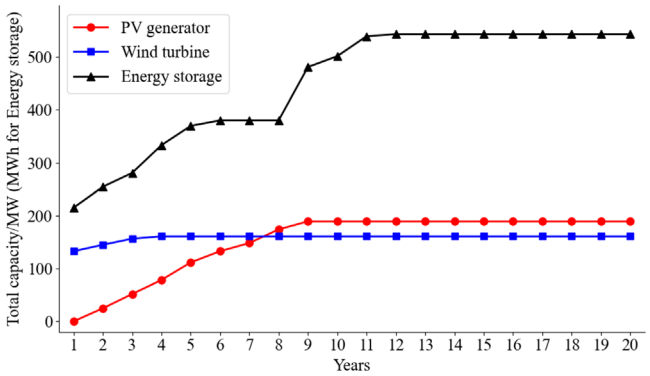

FIGURE 10 | Optimal capacity plan for the balanced wind-solar region.

The plan for the wind-dominant region involves a substantial upfront investment in wind turbine (379.3 MW in Year 1), increasing to 390.3 MW by Year 3. Investment in the PV generator is minimal and deferred until Year 7, reaching only 30.9 MW by Year 9. Energy storage is deployed in phases: 107.8 MWh in Year 1, increasing to 196.3 MWh by Year 5, and finally reaching 424.1 MWh by Year 11, resulting in a storage-to-generation ratio close to 1:1. This strategy resembles the original SGLS project's optimal plan in Section 3.1 due to the shared wind-dominant characteristic. However, the higher capacity factor of the simulated wind farm (0.36 vs. 0.28) makes wind investment even more attractive, leading to greater capacity of the wind turbine and less capacity of the PV generator compared to the base case.

3. **Balanced Wind-Solar Region**: A balanced region is simulated using PV Plant 6 and Wind Farm 5, which have similar capacity factors. The optimal plan is shown in Figure 10.

The strategy for the balanced region features an initial wind turbine investment of 132.5 MW in Year 1, gradually increasing to 160.7 MW over 3 years. Investment in PV generator begins in Year 2 and grows annually, reaching 189.1 MW by Year 9, resulting in a near 1:1 wind-to-PV capacity ratio. Energy storage starts at 214.8 MWh in Year 1 and expands to 543.1 MWh by Year 11. The high storage-to-generation ratio (1.55:1) is required to manage the significant variability and intermittency introduced by the substantial share (approx. 50%) of PV generator. The complementary nature of wind and solar resources in this balanced scenario allows for a diversified and resilient generation portfolio.

This section derived optimal capacity plans for the SGLS project under three distinct resource characteristic. In the PV-dominant region, the final wind-to-PV ratio was 0.45:1, necessitating a high energy storage ratio (1.57:1) to manage the PV generator's intermittency. The wind-dominant region prioritized the capacity of wind turbine with energy storage sized at approximately 100% of the generation capacity. The balanced region achieved a nearly 1:1 wind-PV mix, also requiring significant energy storage (1.55:1). Across all scenarios, the capacity of the wind turbine was deployed primarily in the early years. In contrast, PV generator and energy storage were added gradually, consistent with the findings in Section 5.1.

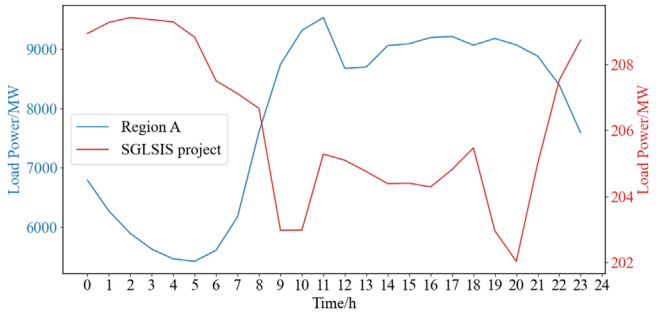

FIGURE 11 | Comparison of average daily load profiles: Region A vs. the SGLS system project.

5.4 | Optimal Capacity Planning Under Different Load Profiles

This section investigates how optimal capacity expansion strategies vary under load profiles with distinct characteristics. The load data are obtained from problem A of the Chinese 9th "Electrician Cup" Mathematical Contest in Modeling, which provides 15-min resolution electric load records for Region A from 1 January, 2009 to 31 December, 2014. Figure 11 compares the average daily load profiles of Region A (2014) and the SGLS project in Section 5.1 (2024).

As shown in Figure 11, in terms of load scale, the average daily load of Region A ranges between 5000 MW and 10,000 MW, which is representative of a provincial-level integrated load. In contrast, the SGLS system project has an average daily load of only 202–209 MW, with a rated load just 3.4% of that of Region A, indicating a small park-level SGLS system project. Regarding load pattern, Region A exhibits a typical grid load profile with distinct morning and evening peaks, and a daily peak-to-valley difference ratio of about 45%, reflecting the influence of social and economic activities. Conversely, the SGLS system project shows a reverse-peak profile: a slight valley during daytime and relatively flat load at night, which is attributed to the utilization of low-cost nighttime wind power. Its daily peak-to-valley difference is only about 3.3%, indicating that this is an industrial load with stable characteristics.

Since Region A represents a provincial-level grid, load growth must be considered. From 2010 to 2014, its annual load growth rates were 11.57%, 6.25%, 3.28%, 4.08%, and 8.19%, respectively, with an average annual growth rate of 6.67% over the 5 years. We assume that the load of Region A continues to grow at 6.67% per year over the next 20 years, and the shape of the added load in each year follows the original profile. Using 2014 as the base year, and to facilitate comparison with the park-level SGLS system project, the load profile of Region A is scaled proportionally so that its peak load matches the rated capacity of the project (340 MW). Wind/PV output and electricity price data in the base year are the same as those of the SGLS system project, and all other parameters remain consistent. The technology cost reduction pathway follows the base case. Figure 12 presents the optimal capacity expansion pathway for Region A under the wind and solar resource endowment of the SGLS system project.

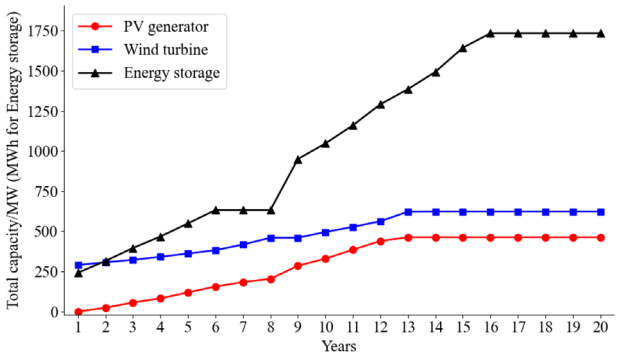

FIGURE 12 | Optimal capacity expansion for Region A.

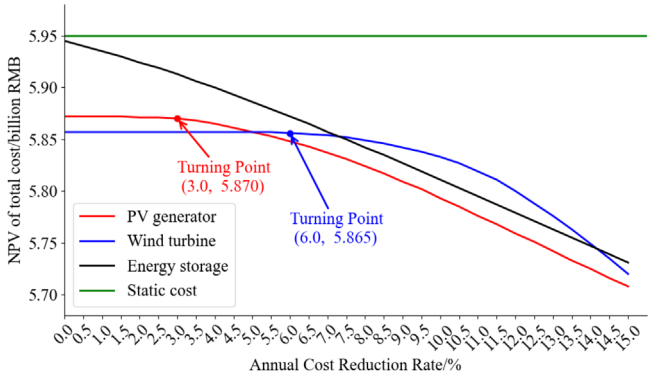

FIGURE 13 | Sensitivity analysis of annual cost reduction rates on the NPV.

Figure 12 shows that, due to continuous load growth over the planning horizon, the cumulative installed capacities of wind turbine, PV generator, and energy storage in Region A also increase steadily. In the first year, 290.2 MW of wind turbine and 242 MWh of energy storage were installed, while no PV generator was installed. By year 13, capacities of wind turbine and PV generator stabilize at 622.8 MW and 462.6 MW, respectively, yielding a wind-to-PV ratio of 1.35:1. The energy storage capacity increases from 242 MWh in the first year to 1733.9 MWh in year 16, a 616% growth. The final ratio of the capacity of energy storage to generation capacity reaches 1.6:1.

Compared with the optimal expansion pathway of the SGLS system project in Section 3.1, wind power remains the dominant source under the Region A load profile, but the share of the PV generator increases significantly. This is because the load profile of Region A aligns better with the photovoltaic output profile, which improves the utilization rate and capacity factor of the PV generator. Moreover, the ratio of energy storage capacity to generation capacity is about 1:1 in the original SGLS system project, but increases to 1.64:1 under the Region A load. This can be attributed to two factors: first, the higher daily peak-to-valley difference (about 45%) in Region A requires greater energy storage capacity to shave the peak load; second, the increased PV generator penetration necessitates additional energy storage to mitigate the variability and intermittency of solar power.

5.5 | Sensitivity Analysis

This section conducts a sensitivity analysis on the annual cost reduction rates of PV generator, wind turbine, and energy storage investments in the optimization model. Based on the previously defined base scenario, a single-factor sensitivity analysis is performed: for each parameter variation, only one cost reduction rate is altered while the other two remain fixed at their base values, and the optimization model is re-run to systematically evaluate its impact on the NPV of the total system cost. The annual cost reduction rates for the three technologies vary from 0% to 15%, with a step size of 0.5%. This range covers scenarios from technological stagnation (0%) to breakthrough progress (15%), ensuring the comprehensiveness of the sensitivity analysis. Figure 13 illustrates the impact of the three annual cost reduction rates on the NPV of the total cost.

As shown in Figure 13, the NPV of the total cost decreases as the annual cost reduction rates of PV generator, wind turbine, and energy storage increase. In other words, faster cost reductions lead to more significant life-cycle cost savings. Among the three technologies, the cost reduction of energy storage has the most pronounced impact on system economics. When its annual reduction rate increases from 0% to 15%, the total cost NPV decreases from 5.945 billion RMB to 5.731 billion RMB. This implies that for every 1% increase in the annual cost reduction rate of energy storage, the total cost NPV is reduced by approximately 0.014 billion RMB. Moreover, starting from 0%, the total cost NPV shows a significant linear decreasing trend with no obvious turning point, indicating that even minor cost improvements in energy storage technology yield immediate economic benefits.

In contrast, wind turbine and PV generator cost reductions exhibit clear turning points. For wind turbine, a noticeable marginal benefit on project cost only emerges after the annual reduction rate reaches 6%. Beyond this threshold, each 1% increase in the cost reduction rate wind turbine reduces the total cost NPV by about 0.015 billion RMB, with marginal benefits increasing as the rate rises. For PV generator, cost reduction effects become apparent only after the annual rate exceeds 3.0%. Beyond that, each 1% increase in the cost reduction rate of the PV generator lowers the total cost NPV by approximately 0.0135 billion RMB.

Additionally, when the annual cost reduction rates for wind turbine and PV generator are 0%, the total costs are 5.857 billion RMB and 5.872 billion RMB, respectively. When the cost reduction rate of energy storage is 0%, the total cost is 5.945 billion RMB, which is only 0.08% higher than the NPV under static costs.

In summary, reductions in energy storage costs are the primary driver of economic performance for this park-level SGLS project. It is recommended that SGLS projects prioritize lowering costs of energy storage. Cost reductions of wind turbine and PV generator only significantly improve project economics after reaching 6% and 3%, respectively.

6 | Conclusions

This study develops a multi-period source-storage coordinated planning model for SGLS system projects, improving the economic efficiency by leveraging the wind-solar complementarity,

dynamic investment cost, and self-declared capacity. The case studies demonstrate significant practical value of the proposed approach via three principal findings:

1. The model achieves substantial cost reductions compared to a real-world SGLS project, with total life-cycle costs decreasing by 7.54%–9.67% and capacity costs decreasing by approximately 7.6%. Electricity purchasing decreases by approximately 50% in peak periods and increases by about 35% during valley periods, with the maximum purchasing electricity reduced by 10%, reflecting the model's grid-friendliness. Investment timing shows distinct patterns: deployments of energy storage and PV generator are deferred under faster cost declines, while investments in wind turbine remain front-loaded due to lower cost sensitivity.
2. Optimal capacity planning varies significantly with the characteristic of the resource. PV-dominant regions require high energy storage ratios (1.57:1) to manage intermittency, while provincial-level loads with better solar alignment support higher PV penetration (42.5% vs. 18.9% under industrial loads), necessitating increased capacity of energy storage (1.6:1 vs. 1:1).
3. The reduction in storage investment cost emerges as the primary factor, with each 1% annual rate reduction decreasing the total cost by approximately 0.014 billion RMB through a linear relationship. Investment in wind turbine and PV exhibits threshold effects, becoming significant until exceeding 6% and 3% annual reduction, respectively.

Although the framework provides advanced planning capabilities, future research should address limitations, including impacts of climate variation, nonlinear cost reduction trajectories, uncertainty in market mechanism.

Author Contributions

Yuankang He: data curation, formal analysis, methodology, writing – original draft. **Zijun Mao**: methodology, software, visualization, data curation, visualization, writing – original draft **Hongxing Ye**: conceptualization, methodology, funding acquisition, project administration, supervision, writing – review and editing.

Funding

This work was supported by State Grid of China Science and Technology Project (No. 5100-202456011A-1-1-ZN).

Conflicts of Interest

The authors declare no conflicts of interest.

Data Availability Statement

The data that supports the findings of this study are available on request from the corresponding author. The data is not publicly available due to privacy or ethical restrictions.

References

1. M. Hand, T. Mai, S. Baldwin, et al., *Renewable Electricity Futures Study - Volume One* (National Renewable Energy Laboratory, 2016).

2. Z. Zhuo, N. Zhang, J. Yang, et al., "Transmission Expansion Planning Test System for AC/DC Hybrid Grid with High Variable Renewable Energy Penetration," *IEEE Transactions on Power Systems* 35, no. 4 (2020): 2597–2608.

3. J. Wang, P. P. Zeng, L. Yin, Y. Dong, X. Liu, and R. Yang, "A Two-Stage Distributed Stochastic Planning Method for Source-Grid-Load-Storage Flexibility Resources Considering Flexible Ramp Capacity," *International Journal of Electrical Power & Energy Systems* 160 (2024): 110134, https://www.sciencedirect.com/science/article/pii/S0142061524003557.

4. X. Guo, J. Zhou, L. Wang, S. Zhang, and J. Geng, "Calculation Method of System Reserve Capacity Considering New Energy Uncertainty in Source-Grid-Load-Storage Scheduling Mode," in *2022 IEEE 6th Conference on Energy Internet and Energy System Integration (EI2)* (IEEE, 2022), 2761–2766.

5. G. Xiaorui, Z. Xiang, M. Zhiquan, W. Ke, G. Jian, and W. Liwen, "Research on the Key Technology Framework of Collaborative Optimization Decision-Making for Highly Resilient Power Grid," in *2021 International Conference on Power System Technology (POWERCON)* (IEEE, 2021), 471–476.

6. S. Xia, Y. Wang, X. Hu, et al., "Source-Network-Load-Storage Collaborated Two-Stage Power Dispatch of Active Distribution Network with Conditional Value-at-Risk," *International Journal of Electrical Power & Energy Systems* 172 (2025): 111120, https://www.sciencedirect.com/science/article/pii/S0142061525006684.

7. W. Li, J. Wang, E. Du, P. Wang, N. Zhang, and C. Kang, "Planning Coal Power Generation Transition Considering Multiple Alternatives With a Full Life Cycle Perspective," *IEEE Transactions on Power Systems* 40, no. 6 (2025): 5171–5183.

8. F. Bu, Y. Wang, S. Zhang, and S. Chen, "Optimization of Source-Grid-Load-Storage Coordinated Energy System for Low-Carbon Community," in *2022 IEEE 6th Conference on Energy Internet and Energy System Integration (EI2)* (IEEE, 2022), 240–245.

9. T. Zhang, D. Yue, L. Yu, C. Dou, and X. Xie, "Joint Energy and Workload Scheduling for Fog-Assisted Multimicrogrid Systems: A Deep Reinforcement Learning Approach," *IEEE Systems Journal* 17, no. 1 (Mar. 2023): 164–175, https://ieeexplore.ieee.org/document/9778182.

10. R. Atia and N. Yamada, "Sizing and Analysis of Renewable Energy and Battery Systems in Residential Microgrids," *IEEE Transactions on Smart Grid* 7, no. 3 (2016): 1204–1213.

11. X. Chen, W. Dong, and Q. Yang, "Robust Optimal Capacity Planning of Grid-Connected Microgrid Considering Energy Management Under Multi-Dimensional Uncertainties," *Applied Energy* 323 (2022): 119642, https://www.sciencedirect.com/science/article/pii/S0306261922009436.

12. L. Yi, J. Meng, and C. He, "Source-Grid-Load-Storage Robust Coordinated Planning of New-Type Power System Considering Primary Frequency Response Characteristics," *Dianwang Jishu/Power System Technology* 47, no. 9 (2023): 3659–3668.

13. M. H. S. Boloukat and A. A. Foroud, "Stochastic-Based Resource Expansion Planning for a Grid-Connected Microgrid Using Interval Linear Programming," *Energy* 113 (2016): 776–787, https://www.sciencedirect.com/science/article/pii/S0360544216310222.

14. A. Khodaei, S. Bahramirad, and M. Shahidehpour, "Microgrid Planning Under Uncertainty," *IEEE Transactions on Power Systems* 30, no. 5 (2015): 2417–2425.

15. M. Yin, K. Li, and J. Yu, "A Data-Driven Approach for Microgrid Distributed Generation Planning Under Uncertainties," *Applied Energy* 309 (2022): 118429, https://www.sciencedirect.com/science/article/pii/S0306261921016561.

16. X. Cao, J. Wang, and B. Zeng, "A Chance Constrained Information-Gap Decision Model for Multi-Period Microgrid Planning," *IEEE Transactions on Power Systems* 33, no. 3 (2018): 2684–2695.

17. B. Ma, X. Li, Q. Tan, and F. Li, "Multi-Objective Multi-Stage Distributionally Robust Chance-Constrained Low-Carbon Planning Model for a Novel Integrated Multi-Energy Microgrids Incorporating Data Center

Considering Real-Time Workload Response and Multiple Uncertainties," *Energy* 332 (2025): 137110, https://www.sciencedirect.com/science/article/pii/S0360544225027525.

18. Z. Shen, P. Li, R. Shi, Z. Xia, and G. Wang, "Optimization Allocation Strategy of Distributed Generation in Grid-Connected Microgrid Based on Economic Dispatch," in *2021 IEEE 5th Conference on Energy Internet and Energy System Integration (EI2)* (IEEE, 2021), 4398–4403.

19. Z. Xia, P. Li, Y. Ji, Z. Shen, and G. Wang, "Optimal Configuration of Grid-Connected Microgrid Considering Real-Time Electricity Price," in *2021 IEEE 5th Conference on Energy Internet and Energy System Integration (EI2)* (IEEE, 2021), 4404–4410.

20. S. Xiang, D. Xu, P. Wang, Z. Bai, and L. Zeng, "Optimal Expansion Planning of 5G and Distribution Systems Considering Source-Network-Load-Storage Coordination," *Applied Energy* 366 (2024): 123372, https://www.sciencedirect.com/science/article/pii/S0306261924007554.

21. A. J. Conejo, Y. Cheng, N. Zhang, and C. Kang, "Long-Term Coordination of Transmission and Storage to Integrate Wind Power," *CSEE Journal of Power and Energy Systems* 3, no. 1 (Mar. 2017): 36–43, https://ieeexplore.ieee.org/abstract/document/7874619.

22. N. Zhang, H. Jiang, E. Du, et al., "An Efficient Power System Planning Model Considering Year-Round Hourly Operation Simulation," *IEEE Transactions on Power Systems* 37, no. 6 (Nov. 2022): 4925–4935, https://ieeexplore.ieee.org/document/9695353/authors.

23. N. Zhang, Z. Hu, B. Shen, S. Dang, J. Zhang, and Y. Zhou, "A Source–Grid–Load Coordinated Power Planning Model Considering the Integration of Wind Power Generation," *Applied Energy* 168 (Apr. 2016): 13–24, https://www.sciencedirect.com/science/article/pii/S0306261916300733.

24. Q. Tan, X. Li, W. Fan, H. Wang, and J. Yang, "Some Key Issues in Building a "Source Network Load Storage" Complementary Energy Internet in China," *Environmental Science and Pollution Research* 30, no. 35 (July 2023): 83513–83529, https://doi.org/10.1007/s11356-023-28284-4.

25. J. Chen, "Solar and Wind Power Data from the Chinese State Grid Renewable Energy Generation Forecasting Competition," *Scientific Data* 9 (2022): 577.